

Peyman Davvalo Khongar

Department of Civil,
Chemical and Environmental Engineering,
University of Genoa,
Genoa 16145, Italy
e-mail: peyman.davvalo.khongar@edu.unige.it

Jan Oscar Pralits

Department of Civil,
Chemical and Environmental Engineering,
University of Genoa,
Genoa 16145, Italy
e-mail: jan.pralits@unige.it

Paolo Soleri

Ophtec BV,
Groningen 9728 NR, The Netherlands
e-mail: p.soleri@ophtec.com

Mario Romano

Department of Biomedical Sciences,
Humanitas University,
Rozzano,
Milano 20090, Italy
e-mail: mario.romano@hunimed.eu

Rodolfo Repetto

Department of Civil, Chemical and
Environmental Engineering,
University of Genoa,
Genoa 16145, Italy
e-mail: rodolfo.repetto@unige.it

A Study of the Mechanical Forces on Aphakic Iris-Fixated Intraocular Lenses

Iris-fixated aphakic intraocular lenses (IFIOL) are used in cataract surgery when more common intraocular lenses (IOL) cannot be adopted because of the absence of capsular bag support. These lenses can be implanted on either the posterior or the anterior surface of the iris. In this work, we study whether one of these options is preferable over the other from the mechanical point of view. In particular, we focus on the forces that the IFIOL transmits to the iris, which are associated with the risk of lens dislocation. We study the problem numerically and consider aqueous flow induced by saccadic rotations in the cases of an IFIOL in the anterior and posterior sides of the iris. The considered IFIOL is the Artisan Aphakia +30.0 D lens (IFIOL) produced by Ophtec BV. We perform the simulations in openFOAM. We find that the forces transmitted by the aphakic IFIOL to the iris are significantly higher in the case of posterior implantation. This suggests that lens implantation on the posterior surface of the iris might be associated with a higher risk of lens dislocation, when an inadequate amount of iris tissue is enclavated during implantation. [DOI: 10.1115/1.4040588]

1 Introduction

Cataract is a process of progressive loss of the transparency, or clouding, of the crystalline lens in the eye, which leads to visual impairment. It is typically associated with aging and it is the major cause, about 50%, of blindness worldwide [1]. The most effective way of treating cataract is surgery and Phacoemulsification is the main current surgical treatment. Phacoemulsification consists in emulsifying the lens with an ultrasonic handpiece and simultaneously aspirating the lens fragments from the eye. The aim of the surgery consists in removing the lens, replacing it with an intraocular lens (IOL) and leaving the elastic capsular bag intact. The IOL is, therefore, placed inside the capsule in order to regain vision.

Posterior capsule rupture (PCR) is one of the most troublesome complications associated with cataract surgery because it leads to loss of capsular support for IOL implantation, disruption of the separation between anterior chamber (AC) and vitreous cavity (VC), and possible dislocation of lens material into the vitreous. This, in turn, can lead to various complications, such as retinal tears and inflammation [2,3]. PCR is not necessarily followed by complete loss of the capsular bag. The incidence of PCR is 2.8%, whereas the incidence of PCR with complete loss of capsular support is about 2% [4].

When the Zonula of Zinn is weak or lost and thus the capsular bag is not able to support the IOL because of degeneration of the ligament or complications occurred during surgery, a secondary implant is required. In such a case, the surgeon often chooses to use an iris-fixated aphakic intraocular lens (IFIOL). These lenses can be positioned either on the anterior or the posterior side of the

iris and are fixated to the relatively immobile midperipheral iris tissue by two rigid haptics, which grasp the iris stroma. The posterior, or retropupillary, implantation technique is gaining popularity, since it is surgically more convenient and it increases the clearance between the IOL and the corneal endothelium, thereby reducing the risk for endothelial cell loss [5].

One of the complications associated with IFIOLs is lens subluxation or dislocation (the two terms will be used interchangeably in the following). While, in the case of retropupillary IFIOL implantation, some studies reported a relatively high prevalence of lens subluxations (e.g., 8.7% [6]; 10% [7]; and 13% [8]), others observed a much smaller frequency or no subluxations at all during the first 4 years postoperative [5,9,10]. Similarly, two studies described that in approximately 6 to 8% of the patients subluxations occurred after anterior implantation of the Artisan Aphakia IOL [11,12]. Several studies proposed that the dislocation or subluxation of the IOLs might be related to the enclavation of an inadequate amount of iris tissue [5,10].

From a mechanical point of view, the IFIOL transmits forces to the iris that are produced by the motion of the surrounding liquid and also by accelerations of the domain. There are several mechanisms creating flow in the eye chambers among which flow induced by eye movements creates higher fluid velocities and, consequently, higher mechanical forces [13–15]. The flow field around the IFIOL is expected to be very different in the case of anterior implantation compared to posterior, thus we anticipate that the forces transmitted to the iris can vary a lot between the two cases. To study this problem, we perform numerical simulations of the flow induced by saccadic rotations in the eye. The aim of the work is to investigate whether eye movements induce forces on the IFIOL, which can play a role in IFIOL subluxation in the case of improper fixation and to compare anterior and

Manuscript received February 21, 2018; final manuscript received June 7, 2018; published online August 20, 2018. Assoc. Editor: Anna Pandolfi.

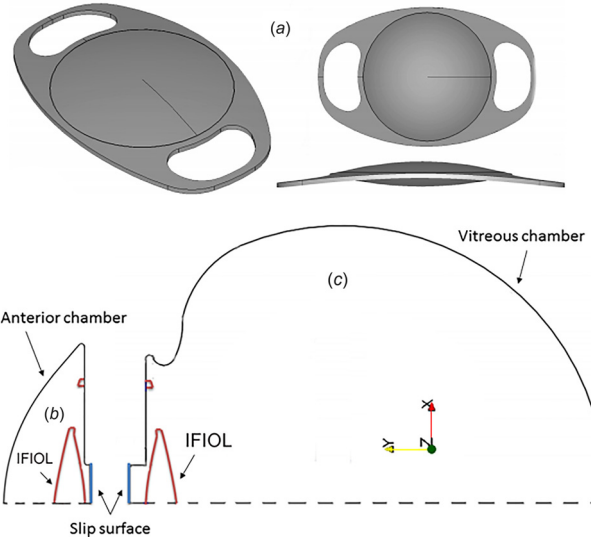


Fig. 1 (a) Different views of the Artisan Aphakia lens. (b) Cross section of the AC with the IFIOL implanted on the anterior surface of the iris. (c) Cross section of the VC with the IFIOL implanted on the posterior surface of the iris. Note that, for graphical reasons, the anterior and vitreous chambers have been moved apart.

retropupillary IFIOL implantation. We consider the Artisan Aphakia +30.0 D IFIOL, designed by Ophtec BV and shown in Fig. 1.

2 Geometries

2.1 The Anterior Chamber. We consider an idealization of the real AC, as shown in Fig. 1(b), which is based on the one used in Repetto et al. [15]. A few modifications were made in order to model the case in which the natural lens has been removed and the iris has moved posteriorly. In particular, in the model [15], the angle between the iris and the cornea was taken to be equal to 30 deg and we increased it in the present analysis. Doing so, the AC depth becomes ≈ 3.14 mm, which is in agreement with the work by Kapnisis et al. [16].

2.2 The Vitreous Chamber. We assume that when the IFIOL is implanted on the posterior surface of the iris, the lens capsule has been removed and vitrectomy has been performed [17]. We assume that after the surgery, all the VC is filled with aqueous. We note that, in some cases, only the anterior portion of the vitreous is removed during the surgery. However, since cataract is typically performed on elderly patients, the vitreous which is left in place is likely to be extensively liquefied, which justifies our choice to model it as a Newtonian fluid.

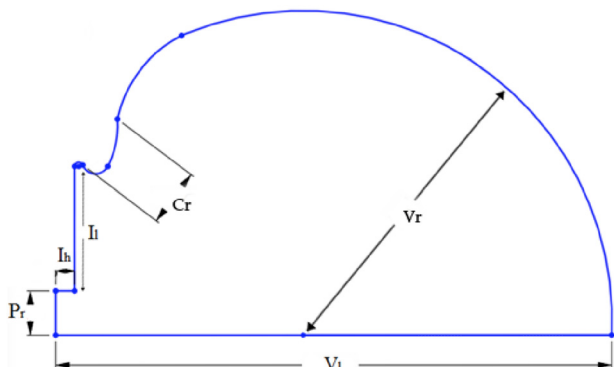


Fig. 2 Cross section of the VC. The values of all parameters are given in Table 1.

Table 1 Values of the geometrical parameters of the VC

Length	Variable	mm	Reference
Ciliary body's length	C_r	2.0	[22,25]
Vitreous chamber radius	V_r	11.0	[22,25]
Vitreous chamber length	V_l	19.5	[22,25]
Pupil radius	P_r	1.5	[15]
Iris length	I_l	5.7	[23]

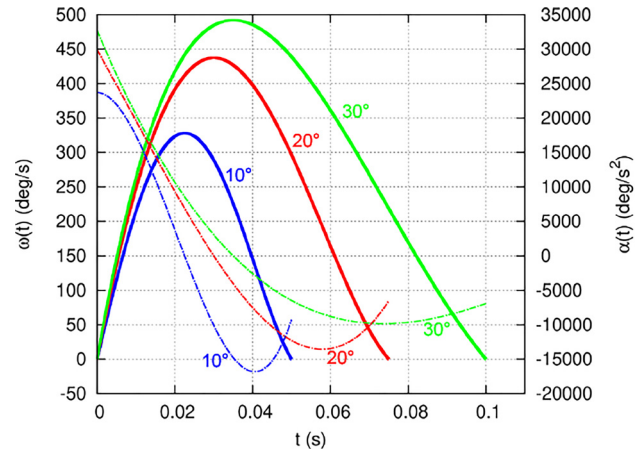


Fig. 3 Angular velocity $\omega(t)$ (solid lines, left vertical axis) and angular acceleration $\alpha(t)$ (dashed-dotted lines, right vertical axis) of saccadic rotations of 10 deg, 20 deg, and 30 deg versus time [14]

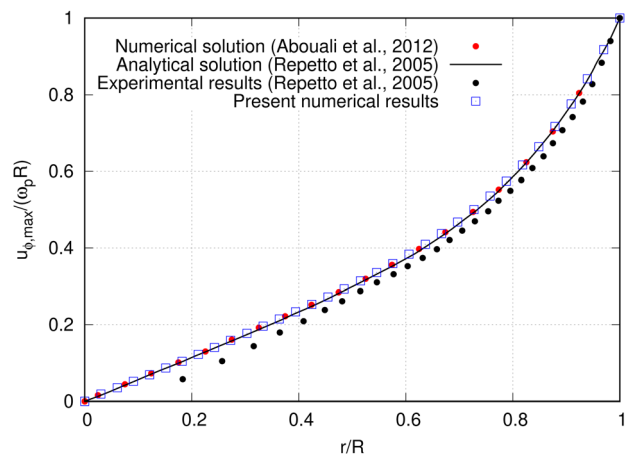


Fig. 4 Validation of the numerical model. Motion of a viscous fluid within a rigid sphere performing a saccadic rotation. Radial profile of the normalized maximum azimuthal velocity $u_{\phi,\max}$. The radial coordinate r is normalized with the sphere radius R . The present numerical findings are compared with the experimental and analytical results of Repetto et al. [14] and with the numerical results of Abouali et al. [28]. We reproduced the conditions of experiment sac-11 in Ref. [14], $R = 0.012$ m, $A = 40$ deg, and $v = 1.4 \times 10^{-4}$ m²/s.

The geometry of the VC used in this work is presented in Fig. 2. We assume that the chamber is axisymmetric, thus neglecting the foveal region, in agreement with many previous works in this field (e.g., see Refs. [18–21]) and we smooth the joints between different tissues. The geometry is based on the works by Worgul [22], Woo et al. [23], and Pavlin et al. [24], and the iris is flattened to be consistent with the shape of the AC, as discussed previously. The values of the parameters introduced in Fig. 2 are reported in Table 1.

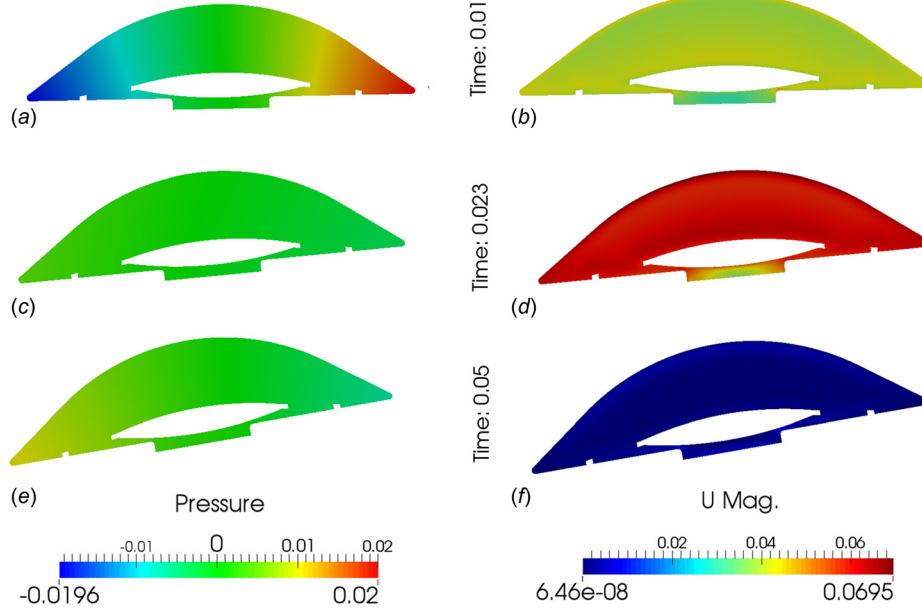


Fig. 5 Maps of the pressure (left) and velocity magnitude (right) in the AC at different times. Saccade with an amplitude of 10 deg. Pressure in Pa and velocity in m/s.

2.3 The Iris-Fixated Aphakic Intraocular Lens. In this study, we consider the Artisan Aphakia lens (+30.0 D), which is shown in Fig. 1(a). The two possible implantation scenarios of the lens (on the anterior or posterior surface of the iris) are shown in Figs. 1(b) and 1(c), respectively.

3 Mathematical Formulation

3.1 Governing Equations. The aqueous humor is treated as an incompressible Newtonian fluid and the governing equations are the Navier–Stokes and continuity equations, which are written and solved with respect to a fixed reference frame

$$\frac{\partial \mathbf{u}}{\partial t} + (\mathbf{u} \cdot \nabla) \mathbf{u} + \frac{1}{\rho} \nabla p - \nu \nabla^2 \mathbf{u} = \mathbf{0} \quad (1a)$$

$$\nabla \cdot \mathbf{u} = 0 \quad (1b)$$

where t is the time, \mathbf{u} denotes the velocity vector, p is the pressure, ρ is fluid density, and ν its kinematic viscosity. We have assumed $\rho = 1000 \text{ kg/m}^3$ and $\nu = 7.5 \times 10^{-7} \text{ m}^2/\text{s}$ [26]. In Eq. (1a), we have neglected gravity, thus the pressure has to be understood as the departure from the hydrostatic pressure distribution.

We solve the above equations in the domains shown in Figs. 1(b) and 1(c). Since the passage of fluid across the pupil during eye rotations is negligible, we perform simulations only in the AC when the IFIOL is implanted on the anterior surface of the iris and only in the VC for posterior lens implantation.

3.2 Eye Rotations and Boundary Conditions. Repetto et al. [14] experimentally investigated fluid motion induced by saccadic eye rotations in an eye model. They suggested to model the eye angular displacement θ of the eyeball in time during a saccade of amplitude A and duration D with the following fifth-order polynomial function:

$$\theta(t) = c_0 + c_1 t + c_2 t^2 + c_3 t^3 + c_4 t^4 + c_5 t^5 \quad (2)$$

The constants c_i ($i=0, \dots, 5$) are determined imposing the following conditions: $\theta(0) = 0$, $\theta(D) = A$, $\dot{\theta}(0) = 0$, $\dot{\theta}(D) = 0$, $\ddot{\theta}(t_p) = \omega_p$, and $\ddot{\theta}(t_p) = 0$, where t_p is the time at which the angular velocity peaks and ω_p is the corresponding peak angular

velocity. Relationships between D , A , t_p , and ω_p are obtained from measurements taken by Becker [27] and also used in Ref. [14].

In Fig. 3, we show the angular velocity and acceleration for amplitudes of 10 deg, 20 deg, and 30 deg, based on such a polynomial function. We note that, in all cases, the initial and final accelerations are nonzero. We use this function to model the motion of the eye, considering amplitudes of 10 deg, 20 deg, and 30 deg. We assume that eye rotations occur about the z -axis in Fig. 1 (pointing up out of the page).

In the numerical simulations, we thus impose the following boundary conditions:

Pupil (blue surface in Fig. 1). The pupil (slip surface in Fig. 1) aperture is not a solid wall and we impose there a slip velocity boundary condition.

All other surfaces. On all other surfaces, we impose the no-slip condition, i.e., the relative velocity of the fluid at the wall, compared to the wall undergoing saccadic motion, is zero.

3.3 Calculation of the Force. The hydrodynamic force on a closed surface S is defined as

$$\mathbf{F} = \int \int_S -p \mathbf{n} dS + \int \int_S \mathbf{d} \mathbf{n} dS \quad (3)$$

where \mathbf{n} is the outer unit normal vector and \mathbf{d} is the deviatoric part of the stress tensor. For the purpose of discussion, we denote the left-hand side $\mathbf{F}_{\text{hydrodynamic}}$, the first integral on the right-hand side as $\mathbf{F}_{\text{pressure}}$ and the second as $\mathbf{F}_{\text{viscous}}$. Since our aim is to calculate the force exerted by the IFIOL on the iris, we also account for the fictitious forces on the lens induced by the acceleration of the domain. These forces are calculated analytically as follows:

$$\mathbf{F}_{\text{fictitious}} = -m\boldsymbol{\Omega} \times (\boldsymbol{\Omega} \times \mathbf{r}) - m \frac{d\boldsymbol{\Omega}}{dt} \times \mathbf{r} \quad (4)$$

where m is the mass of the IFIOL, \mathbf{r} is the distance of the center of mass of the IFIOL from the axis of rotation, and $\boldsymbol{\Omega}$ is the angular velocity. Finally, we denote the total force as $\mathbf{F}_{\text{total}} = \mathbf{F}_{\text{hydrodynamic}} + \mathbf{F}_{\text{fictitious}}$, which represents the force transmitted by the lens to the iris.

3.4 Numerical Solution. The governing Eqs. (1a) and (1b) are solved numerically using the *pimpleDyMFoam* solver in openFOAM v.2.4.¹ This is a large time-step transient solver

¹<http://openfoam.com>

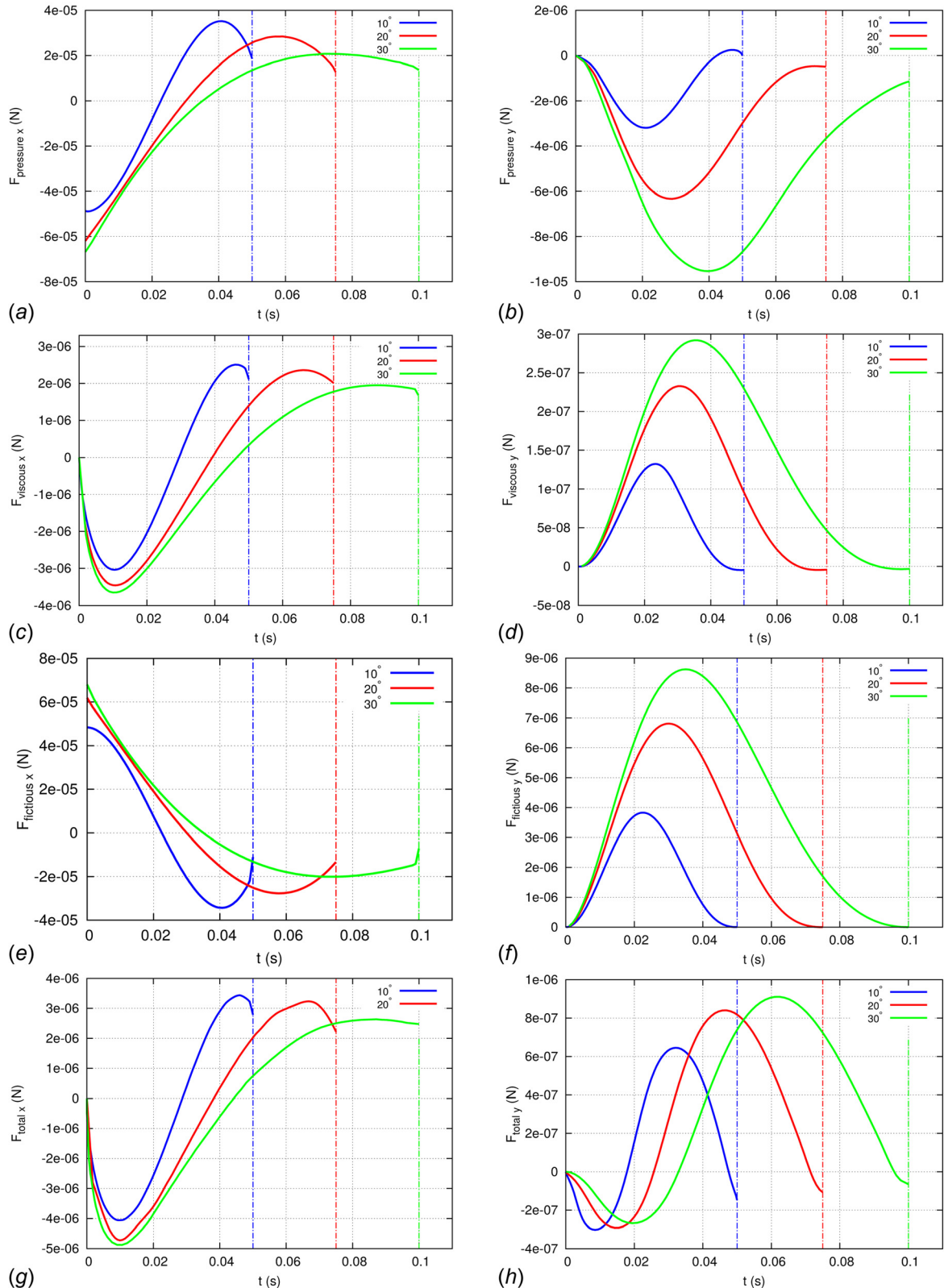


Fig. 6 Various components of the force of the IFIOL on the iris versus time. Left columns: x-component and right column: y-component of the force. Each line corresponds to a Saccade with different amplitudes. The IFIOL is placed on the anterior surface of the iris. Vertical lines mark the time at which saccades end.

for incompressible flows, which considers the dynamical motion of the domain. The hydrodynamic forces on the lens are computed using the force function object utility of openFOAM.

A mesh independence analysis was performed and, for the results presented in this work, a mesh of $\approx 2.5 \times 10^6$ volumes has been used for both the AC and the VC. Moreover, the time-step was fixed to a value of 1×10^{-6} s, with a corresponding maximum

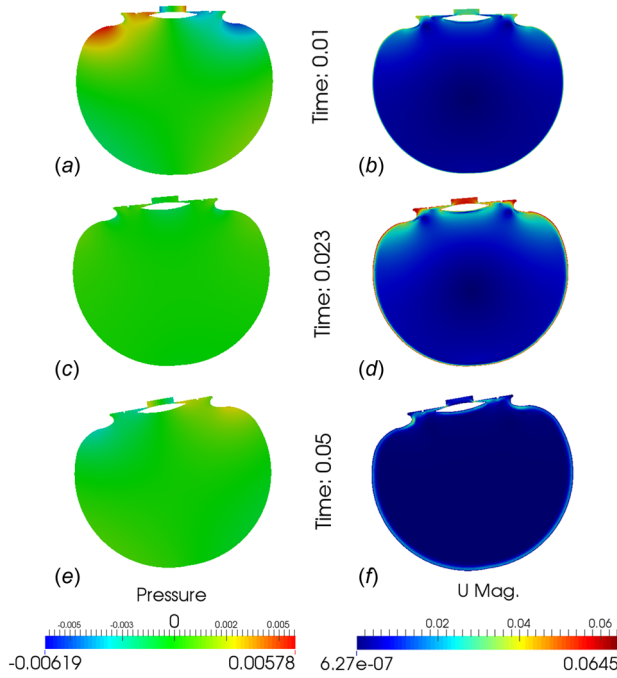


Fig. 7 Maps of the pressure (left) and velocity magnitude (right) in the VC at different times. Saccade with an amplitude of 10 deg. Pressure in Pa and velocity in m/s.

Courant number of 10^{-2} . For all simulations, discretization methods corresponding to second order accuracy in time and space have been adopted.

3.5 Validation of the Numerical Approach. In order to validate our numerical solver, we consider the motion of a viscous fluid within a rigid sphere performing a saccadic rotation about an axis passing through its center. The saccadic motion is described by the law used to obtain Fig. 3. This motion was studied experimentally and theoretically by Repetto et al. [14] and numerically by Abouali et al. [28]. In Fig. 4, we plot the radial profile of the normalized maximum azimuthal velocity $u_{\phi,\max}$. In the figure, the radial coordinate r is normalized with the sphere radius R . The plot shows that our numerical result is in excellent agreement with all previously published data.

4 Results

4.1 Iris-Fixated Aphakic Intraocular Lens Implanted on the Anterior Surface of the Iris. We first consider the case of anterior IFIOL implantation. Figure 5 shows three snapshots of the pressure (left) and velocity distribution (right) in the AC, for the case of a 10 deg saccadic rotation in the counterclockwise direction. At the initial times, Figs. 5(a) and 5(b), the pressure peaks on the right side of the domain, owing to the strong initial angular acceleration. Approximately when the angular acceleration changes sign, Figs. 5(c) and 5(d), the pressure gradient also does so and the maximum of the pressure is localized on the left side of the domain. The saccade motion ends at the time 0.05 s, Figs. 5(e) and 5(f). The figures show that a thin boundary layer forms at the wall, the thickness of which grows in time, owing to viscous diffusion of momentum. After the domain ceases to move ($t \geq 0.05$ s), some fluid motion still occurs in the AC owing to fluid inertia. Much care has been taken to properly resolve with the numerical discretization the thin boundary layer at the wall. This is important since the motion within the boundary layer at the IFIOL surface affects the shear stress exerted on the surface on the lens. Results for 20 deg and 30 deg rotations are not shown since they are qualitatively similar to those presented for the 10 deg case.

We now discuss the forces exerted by the IFIOL on the iris during eye rotations. Even if the governing equations are solved with respect to a fixed reference frame, in terms of absolute velocity, results regarding the forces will be presented with respect to a coordinate system that follows the rotation of the domain. In other words, at all times, the y -axis in Fig. 6 passes through the axis of symmetry of the AC (see also Fig. 1 for orientation of the axes).

In Fig. 6, we report the forces versus time for saccades of 10 deg, 20 deg, and 30 deg. The results show that the force due to the pressure distribution on the IFIOL, $\mathbf{F}_{\text{pressure}}$ (Figs. 6(a) and 6(b)), is larger than the viscous one, $\mathbf{F}_{\text{viscous}}$ (Figs. 6(c) and 6(d)), in all cases. However, the fictitious force, $\mathbf{F}_{\text{fictitious}}$ (Figs. 6(e) and 6(f)), acting on the IFIOL is almost opposite to the force induced by the pressure distribution, so that the sum of the two, Figs. 6(g) and 6(h), turns out to be comparable to the viscous force. The x -component of the pressure and the viscous forces is significantly larger than the y -component for all saccades (by more than an order of magnitude). Correspondingly, also the x -component of $\mathbf{F}_{\text{total}}$ is larger than its y -component for all saccades.

4.2 Iris-Fixated Aphakic Intraocular Lens Implanted on the Posterior Surface of the Iris. In the case of posterior implantation and vitrectomy, the domain is the entire VC, which can be thought of as a deformed sphere. As a consequence, the characteristics of the flow field are expected to be very different from those discussed in Sec. 4.1. In Fig. 7, we report snapshots analogous to those of Fig. 5. As a consequence of the “quasi spherical” shape of the domain, the pressure is almost zero in the core of the domain and attains relatively large values only in the region close to the wall, where the wall velocity has a significant component in the direction normal to the wall specifically in the anterior part of the domain. Relatively large pressures occur in the narrow region between the IFIOL and the iris, even when the domain has come to rest.

The motion remains confined within a narrow boundary layer at the wall, which we took care to properly resolve in the simulations. The velocity out of this thin layer is very small at all times.

A closer inspection of the flow field in the anterior region of the domain shows more complexity (see Fig. 8). A circulation is generated close to the lens, along with further small circulations in the vicinity of the ciliary body. The generation of the large circulation cell behind the IFIOL is consistent with the experimental observations of Stocchino et al. [18] and with the theoretical predictions of Repetto et al. [19]. Indeed, the authors also observed the existence of a circulation in the VC, induced by the change of curvature of the domain produced by the natural lens.

The forces on the lens are reported in Fig. 9. In this case, the x - and y -component of $\mathbf{F}_{\text{pressure}}$ and the x -component of $\mathbf{F}_{\text{viscous}}$ are comparable in magnitude. The x -component of the fictitious force

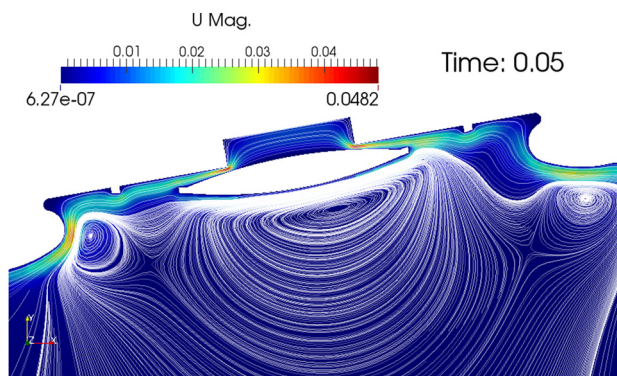


Fig. 8 Map of the velocity magnitude and streamlines in the anterior part of the VC. $t = 0.05$ s, saccade amplitude equal to 10 deg.

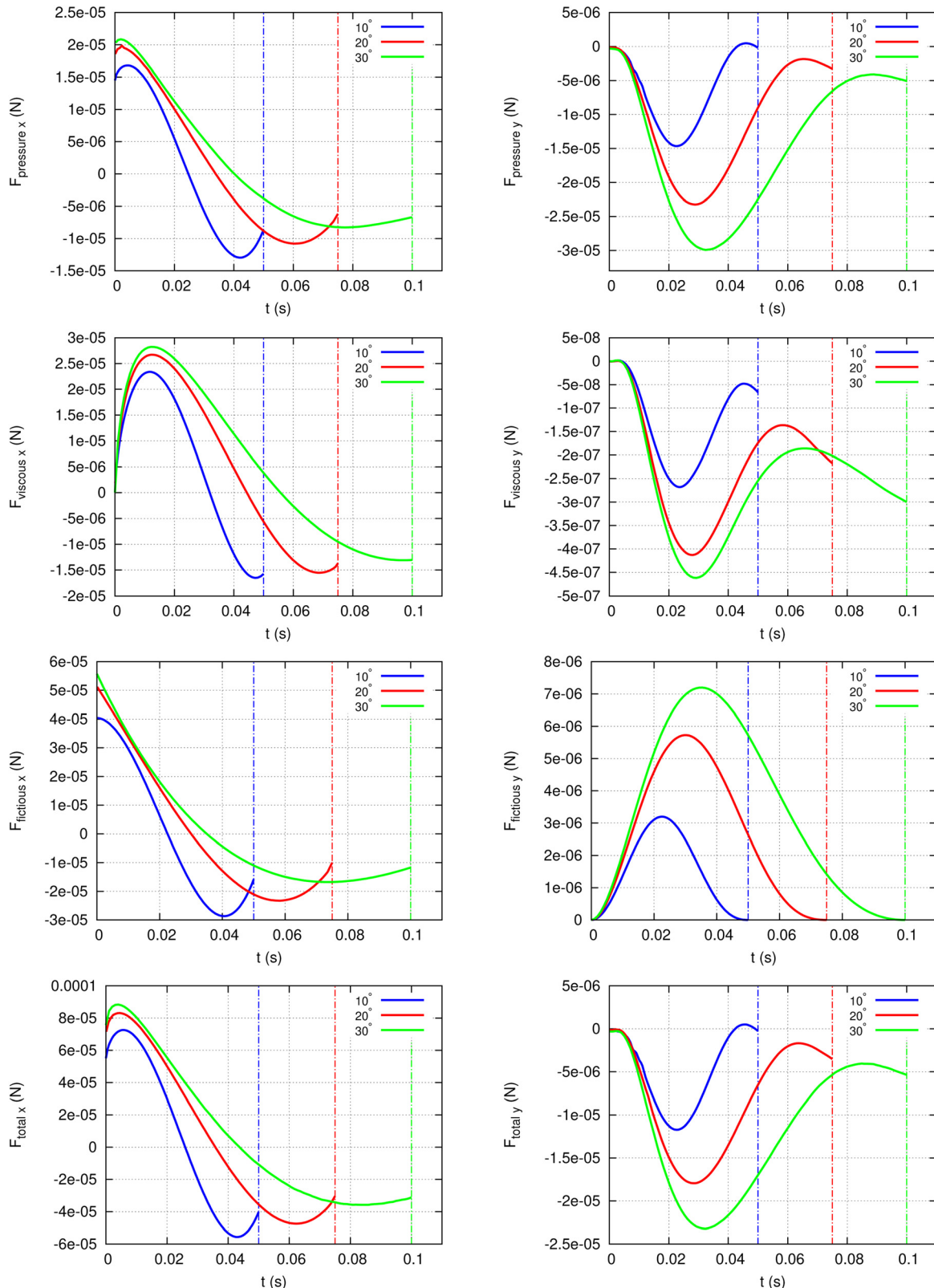


Fig. 9 Various components of the force of the IFIOL on the iris versus time. Left column: x-component and right column: y-component of the force. Each line corresponds to a Saccade with different amplitudes. The IFIOL is placed on the posterior surface of the iris. Vertical lines mark the time at which saccades end.

is, as expected, similar but slightly smaller than that found for the anterior IFIOL implantation, since the center of mass of the IFIOL is in the case of posterior implantation closer to the axis of rotation. We note that the x -component of $\mathbf{F}_{\text{pressure}}$ and $\mathbf{F}_{\text{friction}}$ has the same sign, at almost all times, and therefore sum up.

5 Comparison Between Anterior and Posterior Iris-Fixated Aphakic Intraocular Lens Implantation

In this section, we compare the results obtained for the forces in the case of anterior and posterior IFIOL implantation. In

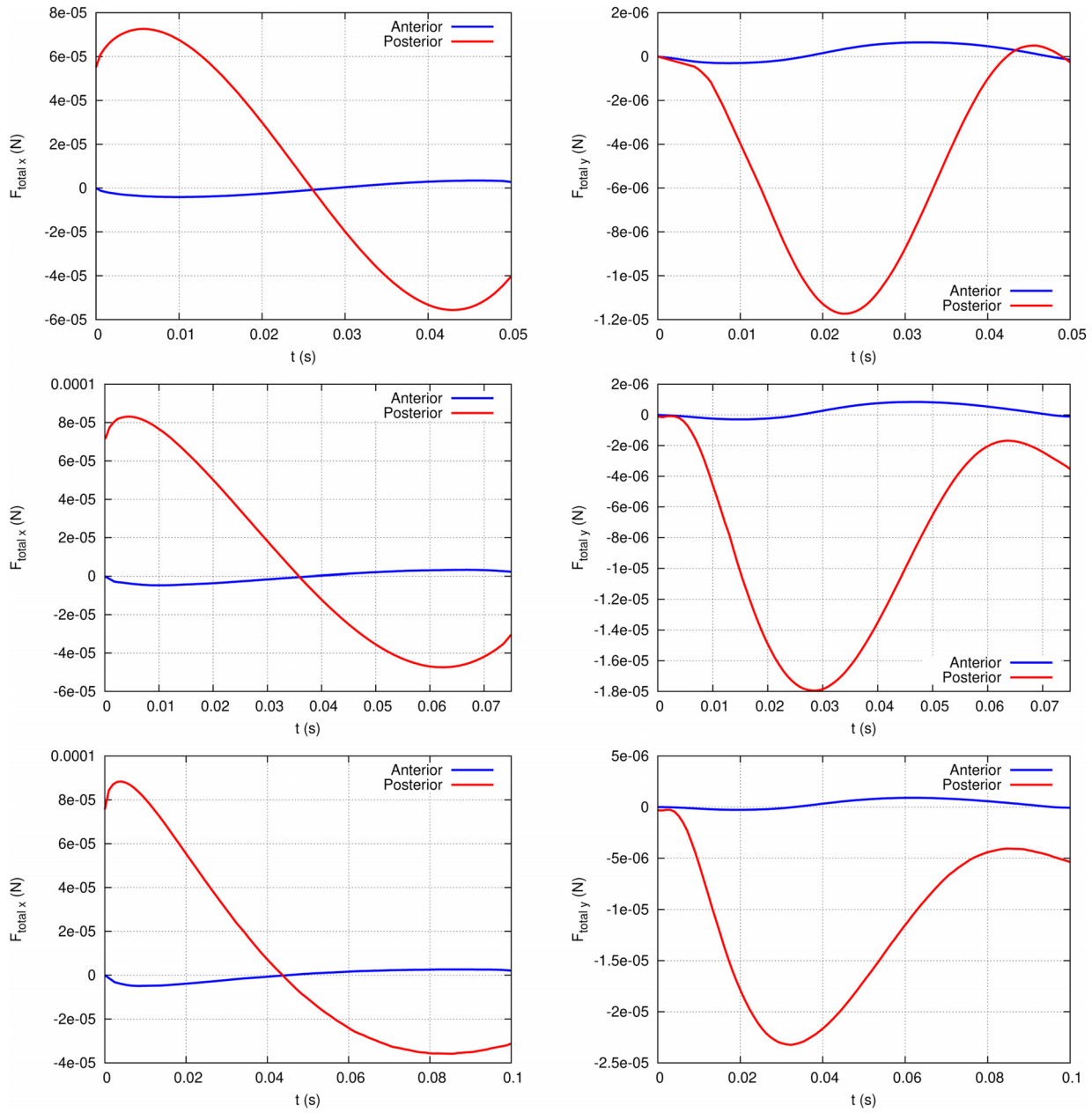


Fig. 10 Total force of the IFIOL on the iris, for the cases of anterior and posterior positioning, versus time. Left column: x-component and right column: y-component of the force. From the top to the bottom, 10 deg, 20 deg, and 30 deg, respectively.

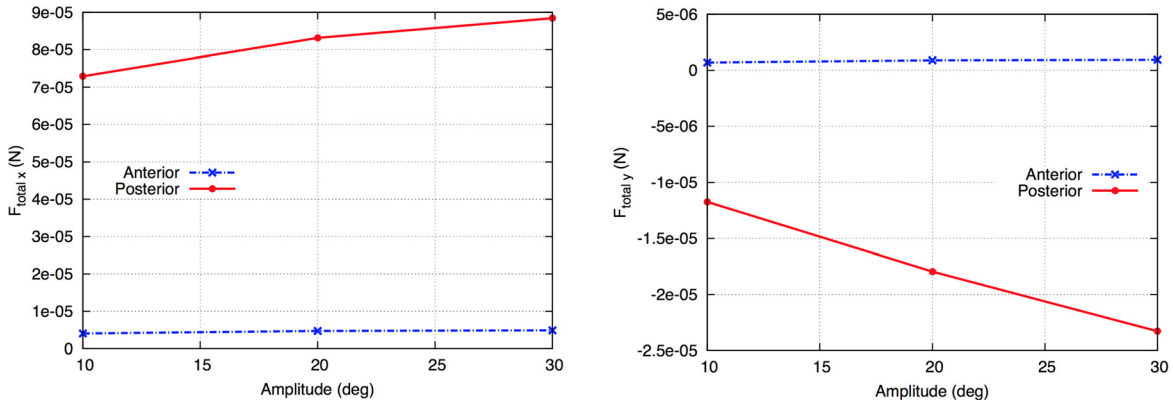


Fig. 11 Maximum force in the x (left) and y (right) directions as a function of the saccade amplitude. For the x-component of the force, we consider the maximum of the absolute value of $F_{\text{total} x}$; for the y direction, we consider the maximum positive value for the dashed-dotted line and the maximum negative value for the solid line.

particular, we compare the values attained by the total force $\mathbf{F}_{\text{total}}$, which is the force transmitted by the IFIOL to the iris. This is an important physical quantity since it is associated with the risk of lens dislocation.

We note that the force in the x -direction can always contribute to lens dislocation, whereas the force in the y -direction (i.e., in the direction approximately orthogonal to the surface of the iris) does so only if it tends to pull the IFIOL away from the iris. This means that, as far as lens dislocation is concerned (what we call in the following detaching force), we only need to consider positive values of $F_{\text{total},y}$ when the lens is placed in the AC and negative values when it is placed behind the iris.

In Fig. 10, we plot the time evolution of the x - and y -component of $\mathbf{F}_{\text{total}}$ for the two cases. The three rows correspond to different amplitudes investigated (10 deg, 20 deg, and 30 deg). The forces are invariably significantly larger (at least by an order of magnitude) when the IFIOL is implanted posteriorly to the iris.

In Fig. 11, we show how the maximum detaching force (in the x - and y -direction) depends on the saccade amplitude. As one might expect, the force grows with the saccade amplitude, the dependency being, however, quite small. This is somehow consistent with the experimental findings of Repetto et al. [14]. The authors showed that the shear stress on the retina only slightly grows with the amplitude of saccades and postulated that small amplitude eye rotations, being much more frequent, could actually be responsible for the possible occurrence of retinal damages.

6 Conclusions

Our results show that the forces transmitted by the IFIOL on the iris are much larger when the IFIOL is mounted on the posterior side, compared to when it is mounted on the anterior side.

In order to understand whether the computed forces are potentially of clinical interest, it is quite natural to compare them with the submerged weight W of the IFIOL, which is the force the IFIOL transmits to the iris in static conditions. This force is not zero, since the lens is not neutrally buoyant and its magnitude can be computed as follows:

$$W = g(m_{\text{IFIOL}} - \rho V_{\text{IFIOL}}) \quad (5)$$

where g is the acceleration of gravity, m_{IFIOL} the mass of the IFIOL (12×10^{-6} kg, information from Ophtec BV), and V_{IFIOL} the IFIOL volume ($V_{\text{IFIOL}} \approx 1.0378 \times 10^{-8} \text{ m}^3$). With the above numbers, we obtain $W = 1.59 \times 10^{-5} \text{ N}$. Comparing the above value with the forces reported in Fig. 11, it appears that W is significantly larger than the forces the IFIOL is subjected to, when it is placed in the AC. On the other hand, when the lens is implanted on the posterior surface of the iris, the dynamic forces generated on the iris during eye rotations are significantly larger than the lens weight W , in particular in the x -direction. Thus, eye rotations certainly have a significant role in the possible dislocation of the lens.

The present study shows a clear difference in the forces induced by eye movements on the iris in the case of anterior or retropupillary IFIOL implantation. In the latter case, the forces transmitted by the haptics to the iris are at least an order of magnitude larger. This, in turn, might increase the risk of subluxation when an inadequate amount of iris tissue is enclavated. Even if there is no clear clinical evidence that retropupillary implantation is associated with a higher prevalence of IFIOL subluxation, the results of this study suggest that a proper fixation is essential to prevent possible subluxations, especially in the case of lens implantation on the posterior surface of the iris.

Acknowledgment

The present work was financially supported by Ophtec BV.

References

- [1] WHO, 2012, "Global Data on Visual Impairments 2010," World Health Organization, Geneva, Switzerland.
- [2] Sparrow, J., Taylor, H., Qureshi, K., Smith, R., Birnie, K., and Johnston, R., 2012, "The Cataract National Dataset Electronic Multi-Centre Audit of 55 567 Operations: Risk Indicators for Monocular Visual Acuity Outcomes," *Eye*, **26**(6), p. 821.
- [3] Hashemi, H., Khabazkhoob, M., Rezvan, F., Etemad, K., Gilasi, H., Asgari, S., Mahdavi, A., Mohazzab-Torabi, S., and Fotouhi, A., 2016, "Complications of Cataract Surgery in Iran: Trend From 2006 to 2010," *Ophthalmic Epidemiol.*, **23**(1), pp. 46–52.
- [4] Ang, G. S., and Whyte, I. F., 2006, "Effect and Outcomes of Posterior Capsule Rupture in a District General Hospital Setting," *J. Cataract Refractive Surg.*, **32**(4), pp. 623–627.
- [5] Forlini, M., Soliman, W., Bratu, A., Rossini, P., Cavallini, G. M., and Forlini, C., 2015, "Long-Term Follow-Up of Retropupillary Iris-Claw Intraocular Lens Implantation: A Retrospective Analysis," *BMC Ophthalmol.*, **15**(1), p. 143.
- [6] Gonnermann, J., Klamann, M. K., Maier, A.-K., Rjasanow, J., Jousseen, A. M., Bertelmann, E., Rieck, P. W., and Torun, N., 2012, "Visual Outcome and Complications After Posterior Iris-Claw Aphakic Intraocular Lens Implantation," *J. Cataract Refractive Surg.*, **38**(12), pp. 2139–2143.
- [7] Rüfer, F., Saeger, M., Nölle, B., and Roider, J., 2009, "Implantation of Retropupillary Iris Claw Lenses With and Without Combined Penetrating Keratoplasty," *Graefe's Arch. Clin. Exp. Ophthalmol.*, **247**(4), p. 457.
- [8] Gonnermann, J., Torun, N., Klamann, M. K., Maier, A.-K. B., Sonnleithner, C. V., Jousseen, A. M., Rieck, P. W., and Bertelmann, E., 2013, "Visual Outcomes and Complications Following Posterior Iris-Claw Aphakic Intraocular Lens Implantation Combined With Penetrating Keratoplasty," *Graefe's Arch. Clin. Exp. Ophthalmol.*, **251**(4), pp. 1151–1156.
- [9] Hazar, L., Kara, N., Bozkurt, E., Ozgurhan, E. B., and Demirok, A., 2013, "Intraocular Lens Implantation Procedures in Aphakic Eyes With Insufficient Capsular Support Associated With Previous Cataract Surgery," *J. Refractive Surg.*, **29**(10), pp. 685–691.
- [10] Schallenberg, M., Dekowski, D., Hahn, A., Laube, T., Steuhl, K.-P., and Meller, D., 2014, "Aphakia Correction With Retropupillary Fixated Iris-Claw Lens (Artisan)-Long-Term Results," *Clin. Ophthalmol.*, **8**, pp. 137–141.
- [11] De Silva, S. R., Arun, K., Anandan, M., Glover, N., Patel, C. K., and Rosen, P., 2011, "Iris-Claw Intraocular Lenses to Correct Aphakia in the Absence of Capsule Support," *J. Cataract Refractive Surg.*, **37**(9), pp. 1667–1672.
- [12] Farrahi, F., Feghhi, M., Maghi, F., Kasiri, A., Afkari, A., and Latifi, M., 2012, "Iris Claw Versus Scleral Fixation Intraocular Lens Implantation During Pars Plana Vitrectomy," *J. Ophthalmic Vision Res.*, **7**(2), p. 118.
- [13] Dyson, R., Fitt, A. J., Jensen, O. E., Mottram, N., Miroshnychenko, D., Naire, S., Ocone, R., Siggers, J. H., and Smithbecker, A., 2004, "Post Re-Attachment Retinal Re-Detachment," Fourth Medical Study Group, University of Strathclyde, Glasgow, Scotland, pp. 1–30.
- [14] Repetto, R., Stocchino, A., and Cafferata, C., 2005, "Experimental Investigation of Vitreous Humour Motion Within a Human Eye Model," *Phys. Med. Biol.*, **50**(19), pp. 4729–4743.
- [15] Repetto, R., Pralits, J. O., Siggers, J. H., and Soleri, P., 2015, "Phakic Iris-Fixated Intraocular Lens Placement in the Anterior Chamber: Effects on Aqueous Flowphakic Iris-Fixated Intraocular Lens Placement," *Invest. Ophthalmol. Visual Sci.*, **56**(5), pp. 3061–3068.
- [16] Kapnis, K., Van Doormaal, M., and Ethier, C. R., 2009, "Modeling Aqueous Humor Collection From the Human Eye," *J. Biomech.*, **42**(15), pp. 2454–2457.
- [17] Hong, A. R., Sheybani, A., and Huang, A. J., 2015, "Intraoperative Management of Posterior Capsular Rupture," *Curr. Opin. Ophthalmol.*, **26**(1), pp. 16–21.
- [18] Stocchino, A., Repetto, R., and Cafferata, C., 2007, "Eye Rotation Induced Dynamics of a Newtonian Fluid Within the Vitreous Cavity: The Effect of the Chamber Shape," *Phys. Med. Biol.*, **52**(7), pp. 2021–2034.
- [19] Repetto, R., Siggers, J., and Stocchino, A., 2010, "Mathematical Model of Flow in the Vitreous Humor Induced by Saccadic Eye Rotations: Effect of Geometry," *Biomech. Model. Mechanobiol.*, **9**(1), pp. 65–76.
- [20] Abouali, O., Modareszadeh, A., Ghaffariyeh, A., and Tu, J., 2012, "Numerical Simulation of the Fluid Dynamics in Vitreous Cavity Due to Saccadic Eye Movement," *Med. Eng. Phys.*, **34**(6), pp. 681–692.
- [21] Modareszadeh, A., and Abouali, O., 2014, "Numerical Simulation for Unsteady Motions of the Human Vitreous Humor as a Viscoelastic Substance in Linear and Non-Linear Regimes," *J. Non-Newtonian Fluid Mech.*, **204**, pp. 22–31.
- [22] Worgul, B. V., 1991, *The Edward S Harkness Eye Institute Resident's Basic Science Study Guide*, Columbia University Press, New York.
- [23] Woo, S. L., Kobayashi, A., Lawrence, C., and Schlegel, W., 1972, "Mathematical Model of the Corneo-Scleral Shell as Applied to Intraocular Pressure-Volume Relations and Applanation Tonometry," *Ann. Biomed. Eng.*, **1**(1), pp. 87–98.
- [24] Pavlin, C. J., Harasiewicz, K., and Foster, F. S., 1992, "Ultrasound Biomicroscopy of Anterior Segment Structures in Normal and Glaucomatous Eyes," *Am. J. Ophthalmol.*, **113**(4), pp. 381–389.
- [25] Gesell, T. F., Hopewell, J. W., Lantz, M. W., Osborne, J. W., Scott, B. R., Seltzer, S. M., Shore, R. E., and Worgul, B. V., 1999, "Biological Effects and Exposure Limits For 'Hot Particles,'" National Council on Radiation Protection and Measurements, Bethesda, MD, NCRP Report No. 130.
- [26] Beswick, J. A., and McCulloch, C., 1956, "Effect of Hyaluronidase on the Viscosity of the Aqueous Humour," *Br. J. Ophthalmol.*, **40**(9), pp. 545–548.
- [27] Becker, W., 1989, "Metrics," *The Neurobiology of Saccadic Eye Movements*, R. Wurtz and M. Goldberg, eds., Amsterdam, The Netherlands.
- [28] Abouali, O., Modareszadeh, A., Ghaffariyeh, A., and Tu, J., 2012, "Investigation of Saccadic Eye Movement Effects on the Fluid Dynamic in the Anterior Chamber," *ASME J. Biomech. Eng.*, **134**(2), p. 021002.